Joint transmission and reflection traveltime tomography in imaging permafrost and thermokarst lakes in Northwest Territories, Canada

JUN-WEI HUANG and GILLES BELLEFLEUR, Geological Survey of Canada

We propose an application of joint tomographic inversion using both transmitted and reflected arrivals to map velocity structures in thick permafrost areas of the Mackenzie Delta, Northwest Territories of Canada. Our tomography algorithm combines a grid-based solver of the eikonal equation, Huygens' principle, and the adjoint method. The grid-based solver assigns a traveltime to each grid point and avoids the shadow-zone problem in classical ray tracing and is well-adapted for parallelization. The adjoint method used in the inversion provides the gradient of a given objective function without explicitly estimating the Fréchet derivative matrix. When combined with Huygens' principle, the tomographic inversion can simultaneously use first and later arrivals to optimize a final velocity model. We first demonstrate the performance of the joint tomography algorithm on a two-dimensional synthetic model with velocity variations typical of permafrost. The method is then applied to a 2D seismic survey covering over 20 km with offsets up to 4 km, acquired in the Mackenzie Delta. The subsurface at that location is characterized by a thick permafrost (600 m) comprising high-velocity and low-velocity areas associated with thermokarst lakes. Our results show the potential of the joint tomography in characterizing multiscale heterogeneous velocity structures within the permafrost.

Introduction

The Mackenzie Delta area is characterized by a remarkable variability in permafrost conditions. In the central Mackenzie Delta, permafrost may be less than 80 m thick whereas in northern Richards Island it may be more than 700 m thick (Judge et al., 1987). This variability in part reflects a complex Quaternary history of surface temperatures and geologic processes (Mackay, 1972; Wyder, 1972; Taylor et al., 1996). In particular, lakes which cover between 20 and 50% of the landscape of the Mackenzie Delta area have played an important role in conditioning ground temperatures. Positive mean annual temperatures beneath the lakes, if imposed for a significant amount of time, can thaw the permafrost and affect the proportion of water versus ice within the sediment matrix. Such variations modify the physical properties of sediments, including the velocity of P-waves which can vary from 1.9 km/s in unfrozen sediments up to 4 km/s in fully frozen sediments (Dallimore et al., 1999). In this paper, we propose to use seismic reflection data to map the permafrost velocity distribution associated with short-wavelength temperature variations due to small-scale thermokarst lakes and long-wavelength structures due to the large-scale variation of permafrost thickness (Trupp et al., 2009).

High-velocity permafrost structures, when present at the surface and within the near surface, can significantly degrade the quality of conventional seismic reflection images of deep geological structures (Riedel et al., 2006). High velocities near or at the surface also tend to confine raypaths followed by direct arrivals, limiting the applicability of first-arrival traveltime tomography to the faster and shallower parts of the permafrost. As a result, these methods cannot provide images of deeper permafrost (often characterized by gradually increasing temperature conditions and decreasing seismic velocity). In this paper, we combine the merits of transmission tomography (also known as turning-ray tomography) with reflection tomography and simultaneously invert for P-wave velocity of shallow and deep permafrost structures. Direct arrivals provide detailed information about the shallower permafrost whereas reflections allow sampling of the deeper permafrost. The method proposed is a grid-based eikonal equation solver that avoids the shadow-zone problems common to conventional ray-tracing methods in heterogeneous media and the adjoint technique that circumvents explicit estimation of a Fréchet derivative matrix which is usually computationally intensive. The joint transmission and reflection traveltime tomography can be performed on parallel computers to handle large-scale surveys or to increase computation efficiency (e.g., Noble et al., 2010). Tests on synthetic and field data demonstrate its potential in characterizing both small- and large-scale velocity structures in permafrost regions.

Methodology: fast sweeping, Huygens' principle and adjoint technique

The eikonal equations appear in many applications, such as optimal control, level set method, image processing, and geometric optics (e.g., Bruss, 1982; Malladi and Sethian, 1996). In seismology, they can be derived from the full elastic wave equation with the high-frequency approximation (Chapman, 2004) as expressed in Equation 1:

$$\left|\nabla T(\mathbf{x})\right|^2 = \frac{1}{c^2(\mathbf{x})} = f^2(\mathbf{x}),\ \mathbf{x} \in \Omega \setminus \Gamma \qquad (1a)$$

with boundary condition

$$T(\mathbf{x}) = g(\mathbf{x}),\ \mathbf{x} \in \Gamma \qquad (1b)$$

where $T(\boldsymbol{x})$ is the traveltime at location $\boldsymbol{x}$, $c(\boldsymbol{x})$ and $f(\boldsymbol{x})$ are the propagation velocity and the slowness, respectively, $\Omega = R^n$ for a n-dimensional problem, and Γ is the boundary with a known function of $g(\boldsymbol{x})$.

Among many grid-based eikonal equation solvers, the fast sweeping method (FSM) (Zhao, 2004) is one implementation that directly discretizes the eikonal equation as a stationary boundary value problem and tracks the wavefront by following the causality of wave propagation. We chose FSM to solve the finite-difference-formulated eikonal equation. Starting from an arbitrary grid, FSM uses an upwind finite-difference scheme to update the traveltime at neighboring grid points following a given order. The upwind scheme considers solutions from

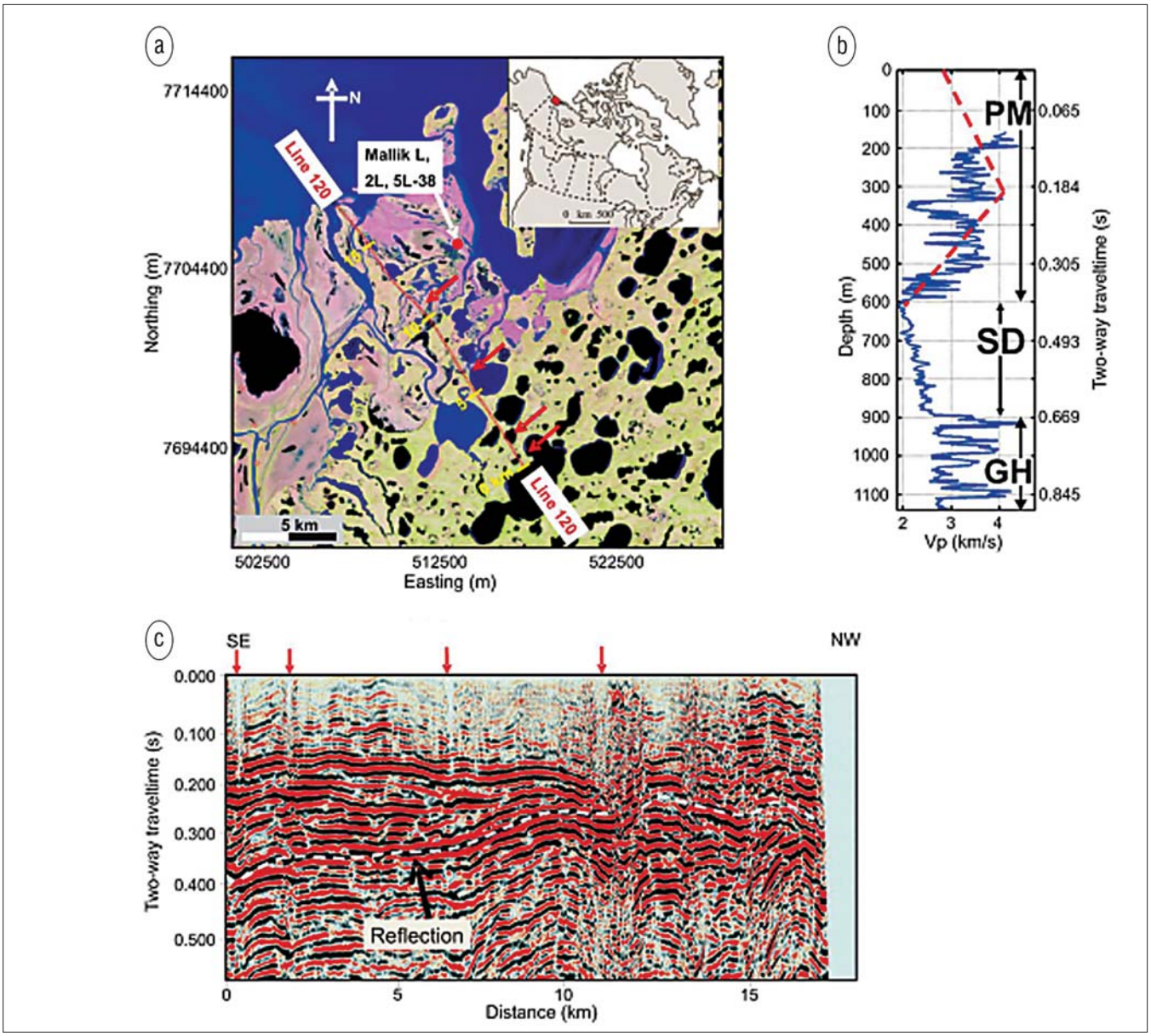

Figure 1. *(a) The 2D seismic survey and well locations on Richards Island, Mackenzie Delta, Northwest Territories of Canada. Line 120 was acquired parallel to the axis of a regional anticline structure and thus is characterized by relatively smooth and shallowly dipping reflection events. Red arrows show water bodies intersected by the profile. (b) P-wave sonic logs measured at Mallik 2L-38 allows the identification of three zones (PM, SD, and GH) representing permafrost, fluid-saturated sediment and gas-hydrate-bearing sediment, respectively (Dallimore et al. 1999). The velocity gradient changes from positive to negative at a depth of 300 m in the permafrost zone. (c) The prestack time-migrated seismic image of line 120. The dashed line marks the reflection used for the joint inversion. The water bodies intersected by the seismic line smear and distort reflections (arrows).*

the direction of propagation of information and maintains the causality of wave propagation in the discretized model. A sweep is completed once the entire model is updated following this order. FSM updates the model using alternating sweeping orders such that each sweep direction covers a class of wave-propagation directions to ensure the causality of wave propagation. The complexity of FSM is in the order of N (the total number of grid points). The accuracy increases linearly with decreasing grid interval (i.e., first-order accuracy) and its implementation is straightforward (Zhao, 2004).

One common disadvantage of grid-based method is that the calculation of secondary arrivals such as reflections is not straightforward. To obtain the later arrivals, we followed the approach of Hole and Zelt (1995) and used Snell's law to update traveltimes by reflected arrivals at the grid points immediately above reflectors. Huygens' principle states that the arrivals along an interface can be used as sources of new wavefronts to track the secondary arrivals. Primary and arbitrary multiple reflection arrival times can be calculated by applying FSM in a "multistage" fashion in which each reflective interface separates the computational domain. This multistage approach is similar to the one proposed by Rawlinson and Sambridge (2004).

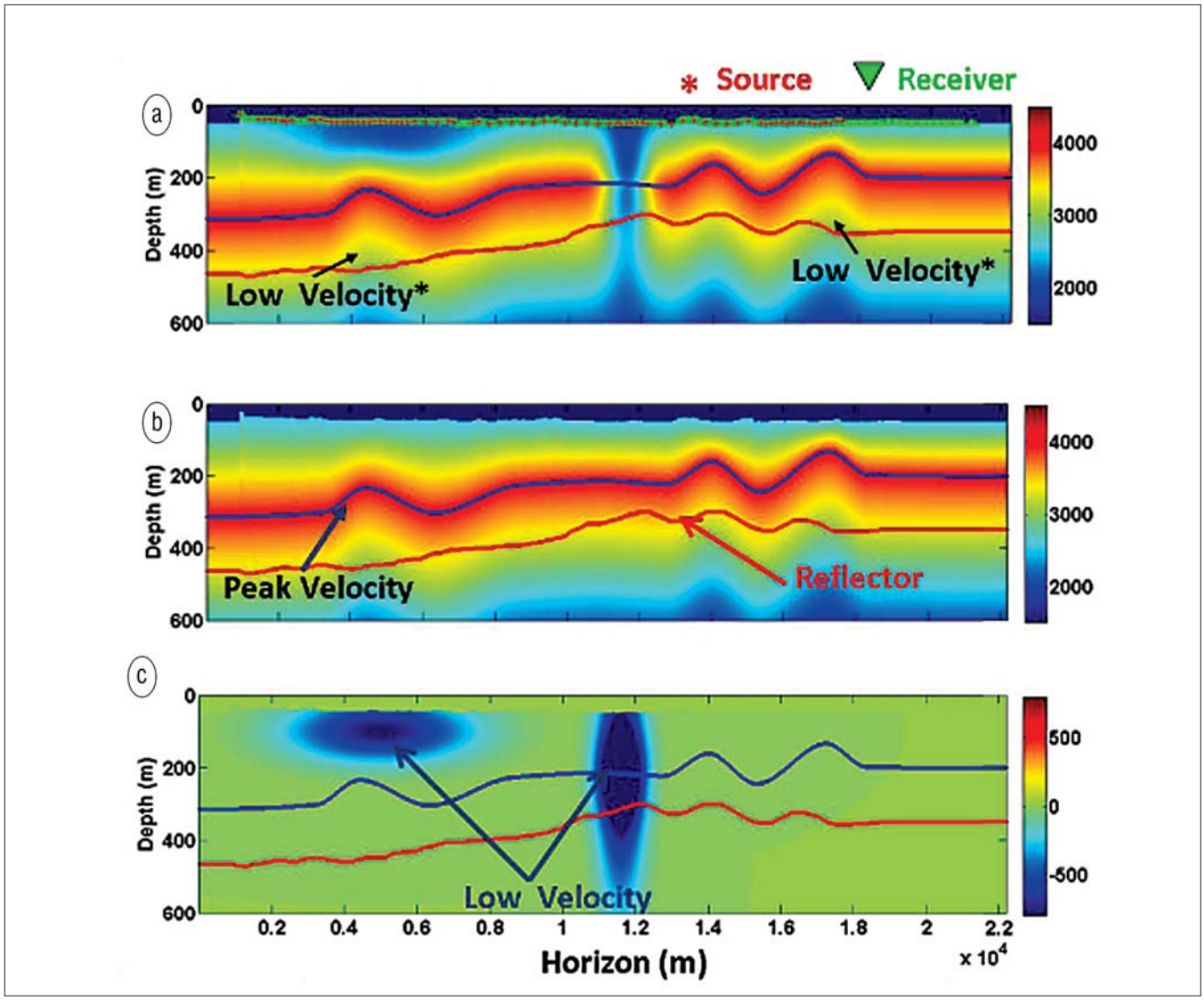

Figure 2. *(a) The true model with the source and receiver locations deployed along a varying topography. (b) The background velocity increases from 2.5 km/s at the surface to 4 km/s at the peak velocity profile and decreases to 2 km/s around a depth of 600 m. It is designed to mimic the velocity trend observed in the Mallik 2L-38 logs. (c) Two low-velocity anomalies representing shallow and deep unfrozen areas within the permafrost. In (a) two extra low-velocity zones above the reflector are caused by some variations in the depth of the peak velocity profile.*

The adjoint method formulates the inverse problem as an optimization problem under the constraint of the partial differential equation (PDE). To avoid the computationally intensive estimation of the Fréchet derivative matrix, a new PDE, termed adjoint PDE, must be solved to obtain the gradient of the misfit function. This turns the inverse problem into another forward modeling problem. The misfit function used in this study is simply the summation of the squared traveltime difference between predicted and observed first and reflection seismic arrivals, and the root-mean-square (rms) misfit is the averaged traveltime residual for each seismic trace.

The mathematical derivations of the adjoint method can be found in Leung and Qian (2006) and a comprehensive review of geophysical applications is given by Plessix (2006). On the practical side, our implementation of the joint transmission and reflection tomography requires traveltimes of first and reflected arrivals and an initial model comprising a velocity distribution and position of interfaces associated with reflected arrivals. The velocity model is updated and optimized to reduce the misfit with direct and reflected traveltimes whereas the position of the reflectors remains static. Two velocity perturbations are simultaneously calculated to reduce the misfit of direct and reflected traveltimes, respectively. The final velocity update is an equal weight summation of the velocity perturbations.

A synthetic case

To test the feasibility of our joint tomography method, we designed a 2D synthetic model providing a representative velocity distribution in a thick permafrost environment and realistic survey geometry based on one 2D profile acquired on Richards Island (line 120 on Figure 1a). In our model, velocity increases with depth to 200–300 m in the shallow subsurface

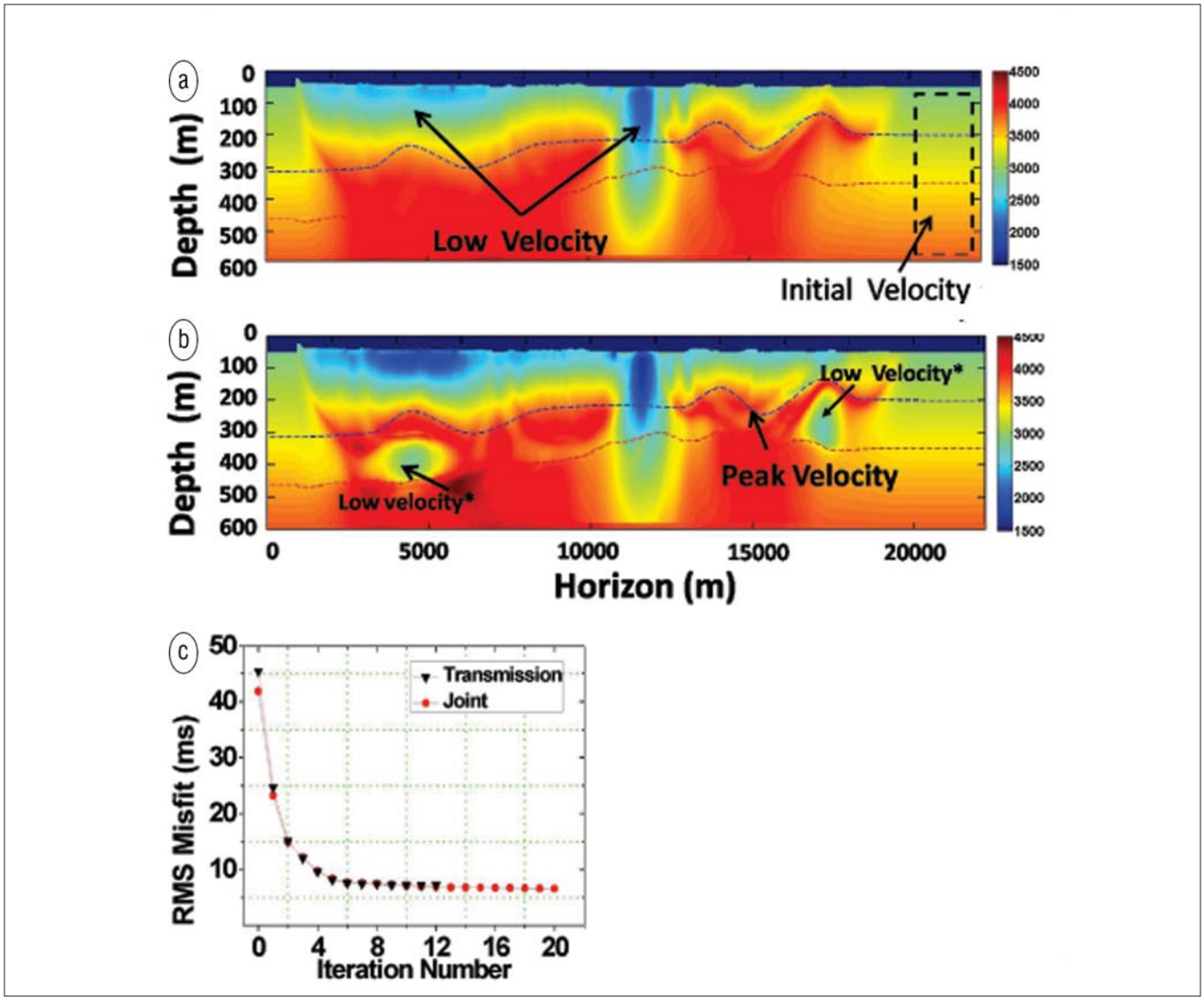

Figure 3. *(a) The final velocity image from turning-ray tomography and (b) from joint tomography from synthetic data. The starting model consists of monotonically increasing velocity with depth and its values can still be observed at the edge of the model. The low-velocity taliks and peak velocity profiles absent in the starting model are better recovered in the joint tomography approach than with turning-ray tomography alone. In particular, the low-velocity regions underlying the peak velocity profile (i.e., the two low-velocity zones in Figure 2a) are also detected by the joint inversion tomography but are slightly stretched due to the limited vertical resolution of reflection arrivals. (c) The rms misfit for the joint and transmission tomography as a function of iteration number is reduced to 5 ms.*

and decreases in the deep part of the permafrost below 300 m (Figure 2b), similarly to a velocity profile obtained from borehole logging data from the Mallik 5L-38 research well (Figure 1b). Two low-velocity anomalies representing shallow and deep unfrozen areas within the permafrost (e.g. taliks) were also introduced in the model (Figure 2c). The final model (Figure 2a) is simply the superposition of the background model (Figure 2b) with the low-velocity anomalies (Figure 2c). We also introduced a seismic reflector in the model representing a change in geological formation. Two low-velocity zones above the reflector (marked with superscript stars in Figure 2a) are due to the topography of the peak velocity distribution and are expected to be sampled by the reflection arrivals. The 2D synthetic acquisition geometry is based on seismic line 120 and has an identical surface topography, and the same distribution of sources and receivers. The synthetic traveltime picks used in the joint inversion are also representative of the frequency of picks made on real data, to ensure that input data are not unrealistically oversampled. Following this, the input traveltime used the same number of transmission and reflection arrivals that could be picked on real data from line 120 (77,220 and 14,862, respectively).

The resulting tomography models after convergence to an optimal solution are displayed in Figure 3, together with the rms misfit as a function of iteration number reaching a plateau of 6 ms. Results obtained with conventional transmission tomography (i.e., using direct arrivals only with FSM and the adjoint method) are shown in Figure 3a whereas results obtained with the joint inversion tomography are shown in Figure 3b. The vertical velocity gradient used as the initial model is still

observable at the edge of the modeling region, where the velocity is hardly sampled by either transmission or reflections (Figure 3b). The peak velocity profile, defined as the velocity gradient turning point, and the low-velocity anomalies, are more accurately modeled and recovered on the joint inversion method (Figure 3b). Overall, the joint inversion tomography enhances the near-surface structures and provides additional details about the deeper permafrost, including low-velocity anomalies such as the deeper part of a talik as well as the low-velocity zones underlying the peak velocity profile.

Field data from permafrost structure on Richards Island

In the winter of 2001, four 2D seismic profiles were acquired by industry on Richards Island in the Mackenzie Delta, where complex thermokarst lakes and heterogeneous permafrost exist in the near surface (Ramachandran et al., 2011). We applied the joint inversion tomography to one of the 2D profiles (line 120) to provide a better understanding of velocity distribution within the permafrost. This seismic profile was designed to avoid major lakes in the area but still intersects some water bodies (marked by arrows in Figure 1). The permafrost near line 120 is approximately 600 m thick (confirmed by industry well-log data). The Mallik 2L-38 gas-hydrate research well (Dallimore et al., 1999) is about 4 km from line 120 (Figure 1a). The effect of lakes (marked in Figure 1a) on the seismic section is observable in Figure 1c, and corresponds to areas where near-surface reflection events lose lateral continuity (marked by arrows). Line 120 is parallel to the crestal plane of an anticline structure and possesses relatively continuous and shallow-dipping reflections, especially on the southeast side of the profile (Figure 1c).

Line 120 comprises 386 shot gathers acquired with 30-m shot and receiver intervals. A total of 77,220 first arrivals with offset up to 4 km were automatically picked, inspected, and manually edited when appropriate. A clear reflection was identified from a prestack time-migrated section (dashed line on Figure 1c) and used in the model after time-to-depth conversion using interval velocities obtained from prestack time-migration velocity analysis. This reflection was also used to define pilot traces to guide the picking of reflection arrivals on unprocessed common midpoint (CMP) gathers. Reflection arrivals at large offset are weak and usually contaminated by noise and thus were not included in the inversion process. A total of 14,862 picks with offset up to 0.5 km were used as input data for reflection traveltimes.

We used the same initial velocity model as in the synthetic test. The results from the joint tomography are shown in Figure 4. In general, the upper part of the final velocity section is mostly controlled by transmission arrivals whereas deeper velocities were updated by reflected arrivals. Results show some similarities with synthetic results. In particular, the zone of peak velocity is well-defined indicating that long-wavelength variations within the permafrost are well-resolved. Some low-velocity anomalies are also well-defined between depths of 0 and 200 m, such as the water bodies marked by arrows in Figure 4a and 4b. In particular, the lowest-velocity anomaly recovered along this profile at 10.5 km corresponds to a highly distorted area on the 2D PSTM stack (Figure 1c) and confirms an imaging problem due to significant lateral velocity variations in the shallow near surface. Velocities beneath this low-velocity anomaly (i.e., beneath the reflector) were not significantly updated during the inversion process, and remained very close to the velocity of the initial model. A high-velocity anomaly is also imaged just below the reflector at approximately 7.5 km in Figure 4b, indicating that joint tomography using both direct and reflected arrivals can locally update the velocity model at depth. This is not necessarily the case elsewhere, as in general no useful velocity information can be obtained below the fixed reflector which is in the lower part of the permafrost. As a result, no velocity information could be recovered close to the base of the permafrost. At the edge of the model area, velocity structures maintained their initial values due to the lack of ray coverage.

Overall, results from the joint inversion of transmitted and reflected arrivals provide additional information that could not be recovered with transmission tomography alone, especially for the deeper parts of the permafrost. However, this method depends strongly on the accurate positioning of the reflector. Inversion results will tend to underestimate the velocity if a reflector is too shallow or overestimate the velocity if it is too deep. Thus, we assumed that this reflector was well-imaged during the prestack time migration and that interval velocities appropriately positioned the reflector at depth.

Conclusion

In this study, we present a joint traveltime-tomography method based on the fast sweeping method, Huygens' principle, and adjoint-state technique. Using the traveltime of transmissions (turning rays) and reflections simultaneously in every step of inversion can mitigate the nonlinearity of inverse modeling, enhance shallow imaging, and reveal deeper structures not visible to turning-ray tomography alone. Our grid-based eikonal equation solver avoids the shadow-zone problems common to conventional ray-tracing methods in a heterogeneous medium and the adjoint technique circumvents explicit estimation of the Fréchet derivative matrix which is usually computationally intensive. The results from synthetic and field data demonstrate its benefits and robustness in recovering both shallow and deep velocity structures in the presence of heterogeneous permafrost and complex thermokarst lakes. The peak velocity profile not present in the starting models is recovered in both synthetic and field data, indicating that long-wavelength variations within permafrost are well-resolved. The images of small-scale low-velocity anomalies corresponding to geologically disturbed areas such as partially frozen lakes are also enhanced by the joint inversion of transmission and reflection traveltimes. TLE

References

ACGR (Associate Committee on Geotechnical Research), 1988, Glossary of permafrost and related ground-ice terms: National Research Council of Canada, Ottawa, Permafrost Subcommittee,Technical Memorandum 142.

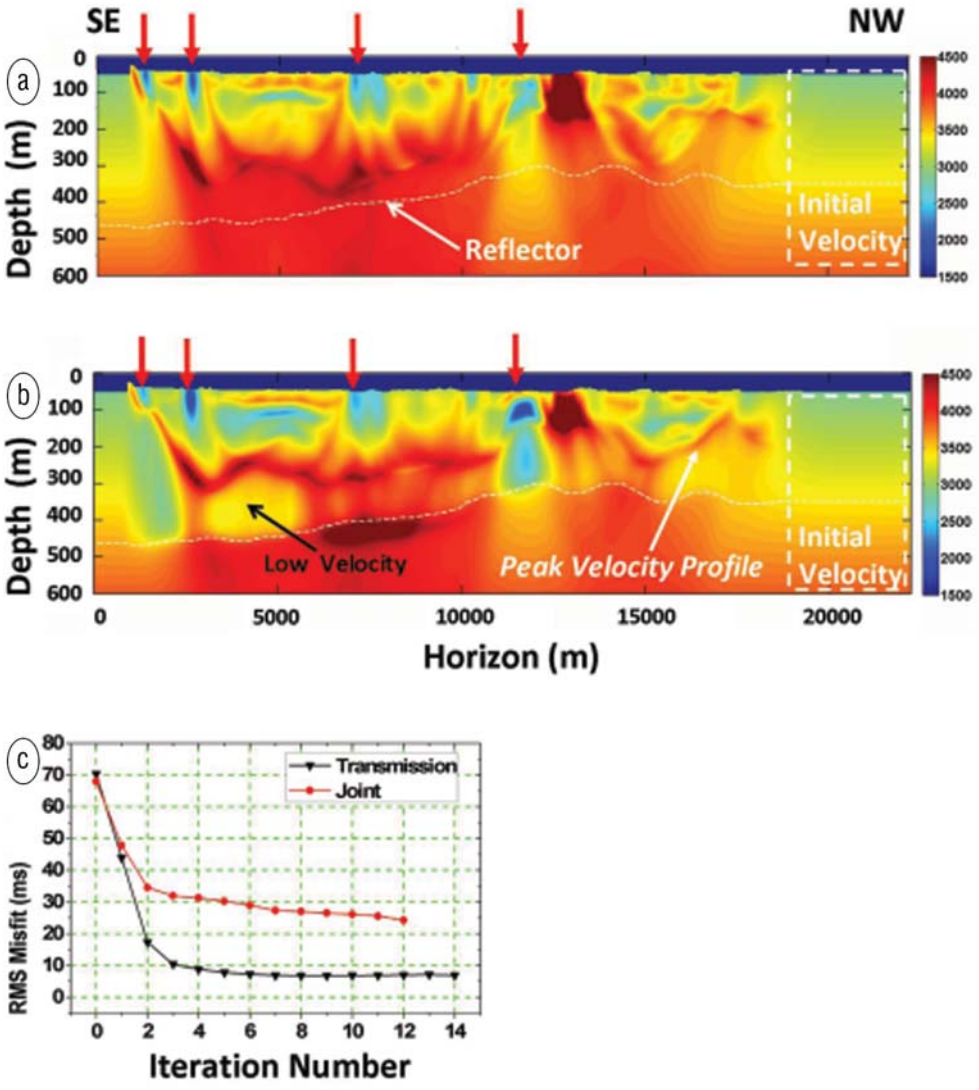

Figure 4. *The final velocity image from (a) first-arrival turning-ray tomography and (b) joint tomography using first and reflected arrivals from line 120. The starting model consisted of monotonically increasing velocity with depth and is still observed on the NW side of the profile. The low-velocity water bodies (arrows) and peak velocity profiles absent in the starting model are well recovered in both tomographic models. The tomographic model from field data shows complicated velocity distribution characterized by various scales and corresponding to water bodies observed on a satellite image (not shown). (c) The rms misfit for the joint and transmission tomography as a function of iteration number is reduced to 21 ms and 7 ms, respectively.*

Bruss, A., 1982, The eikonal equation: Some results applicable to computer vision: Journal of Mathematical Physics, **23**, no. 5, 890–896, doi:10.1063/1.525441.

Chapman, C., 2004, Fundamentals of seismic wave propagation: Cambridge University Press.

Dallimore, S. R., T. S. Collett, and T. Uchida, 1999, Overview of science program, JAPEX/JNOC/GSC et al. Mallik 2L-38 gas hydrate research well, in S.R. Dallimore, T. Uchida, and T.S. Collett, eds, Scientific Results from JAPEX/JNOC/GSC et al. Mallik 2L-38 Gas Hydrate Research Well, Mackenzie Delta, Northwest Territories, Canada: Geological Survey of Canada, Bulletin, **544**, 11–17.

Hole, J. A., and B. C. Zelt, 1995, 3-D finite-difference reflection traveltimes: Geophysical Journal International, **121**, no. 2, 427–434, doi:10.1111/j.1365-246X.1995.tb05723.x.

Judge, A. S., B. R. Pelletier, and I. Norquay, 1987, Permafrost base and distribution of gas hydrates, in B. R. Pelletier, ed., Marine sciences atlas of the Beaufort Sea—geology and geophysics: Geological Survey of Canada Miscellaneous Report 40, 39.

Leung, S. and J. Qian, 2006, An adjoint-state method for three-dimensional transmission traveltime tomography using first-arrivals: Communications in Mathematical Sciences, **4**, 249–266.

Mackay, J. R., 1972, Offshore permafrost and ground ice, Southern

Beaufort Sea: Canadian Journal of Earth Sciences, **9**, 1550–1561, doi:10.1139/e72-137.

Malladi, R., and J. A. Sethian, 1996, A unified approach to noise removal, image enhancement, and shape recovery: IEEE Transactions on Image Processing, **5**, no. 11, 1554–1568, doi:10.1109/83.541425.

Noble, M., P. Thierry, C. Taillandier, and H. Calandra, 2010, High-performance 3D first-arrival traveltime tomography: The Leading Edge, **29**, no. 1, 86–93, doi:10.1190/1.3284057.

Plessix, R.-E., 2006, A review of the adjoint-state method for computing the gradient of a functional with geophysical applications: Geophysical Journal International, **167**, no. 2, 495–503, doi:10.1111/j.1365-246X.2006.02978.x.

Ramachandran, K., G. Bellefleur, T. Brent, M. Riedel, and S. Dallimore, 2011, Imaging permafrost velocity structure using high resolution 3D seismic tomography, Geophysics, **76**, no. 5, doi: 10.1190/GEO2010-0353.1.

Rawlinson, N. and M. Sambridge, 2004, Multiple reflection and transmission phases in complex layered media using a multistage fast marching method: Geophysics, **69**, no. 5, 1338–1350, doi:10.1190/1.1801950.

Riedel, M., G. Bellefleur, T. Brent, S. R. Dallimore, and T. S. Collett, 2006, Amplitude and frequency anomalies in 3D seismic data from the Mallik 5L-38 research site: Geophysics, **71**, no. 6, B183–B191, doi:10.1190/1.2338332.

Taylor, A. E., S. R. Dallimore, and A. S. Judge, 1996, Late Quaternary history of the Mackenzie-Beaufort region, Arctic Canada, from modeling of permafrost temperature, part 2—The Mackenzie Delta-Tuktoyaktuk coastlands: Canadian Journal of Earth Sciences, **33**, no. 1, 62–71, doi:10.1139/e96-007.

Trupp, R., J. Hastings, S. Cheadle, and R. Vesely, 2009, Seismic in arctic environs-Meeting the challenge: The Leading Edge, **28**, no. 8, 936–942, doi:10.1190/1.3192840.

Wyder, J. M., J. A. Hunter, and V. Rampton, 1972, Geophysical investigations of surficial deposits at Tuktoyaktuk, N. W. T: Geological Survey of Canada, Open File 127.

Zhao, H.-K., 2004, A fast sweeping method for Eikonal equations: Mathematics of Computation, **74**, no. 250, 603–627, doi:10.1090/S0025-5718-04-01678-3.

Acknowledgment: BP Canada Energy Company and Chevron Canada Limited kindly provided access to the 2D seismic data from Richards Island (line 120). This is Geological Survey of Canada contribution number 20100473. We appreciate the comments from Bill Goodway, which have improved the readability of the article. Jun-Wei Huang is now with Vibrometric Canada Limited.

Corresponding author: junwei.huang@vibrometric.com